5-28-2019

Nitrogen, Cobalt Co-doped Fluorescent Magnetic Carbon Dots as Ratiometric Fluorescent Probes for Cholesterol and Uric Acid in Human Blood Serum

Shan Huang

Erli Yang

Jiandong Yao

Xu Chu

Yi Liu

See next page for additional authors

Authors
Shan Huang, Erli Yang, Jiandong Yao, Xu Chu, Yi Liu, Yue Zhang, and Qi Xiao

ACS OMEGA

Article

Cite This: ACS Omega 2019, 4, 9333−9342

http://pubs.acs.org/journal/acsodf

Nitrogen, Cobalt Co-doped Fluorescent Magnetic Carbon Dots as Ratiometric Fluorescent Probes for Cholesterol and Uric Acid in Human Blood Serum

Shan Huang,[†,‡] Erli Yang,[†] Jiandong Yao,[†] Xu Chu,[†] Yi Liu,[†] Yue Zhang,[‡] and Qi Xiao*[,†]

[†]Guangxi Key Laboratory of Natural Polymer Chemistry and Physics, College of Chemistry and Materials, Nanning Normal University, 175 Mingxiu East Road, Nanning 530001, P. R. China

[‡]Department of Food Science and Technology, University of Nebraska-Lincoln, 270 Food Innovation Center, Lincoln, Nebraska 68588, United States

Supporting Information

ABSTRACT: Detection of cholesterol and uric acid biomarkers is of great importance for clinical diagnosis of several serious diseases correlated with their variations in human blood serum. In this study, a new kind of well selective and highly sensitive ratiometric fluorescent probe for cholesterol and uric acid determination in human blood serum was innovatively developed on the basis of the inner filter effect (IFE) process of nitrogen, cobalt co-doped carbon dots (N,Co-CDs) with 2,3-diaminophenazine (DAP). DAP was the oxidative product during the oxidation reaction between *o*-phenylenediamine and H_2O_2. Fluorescent magnetic N,Co-CDs possessing blue emission and magnetic property were prepared through a facile one-pot hydrothermal strategy by using citric acid, diethylenetriamine, and cobalt(II) chloride hexahydrate as precursors. N,Co-CDs exhibited good ferromagnetic property and excellent optical properties even in extremely harsh environmental conditions, implying the huge potential applications of such N,Co-CDs in biological areas. On the basis of the IFE process between N,Co-CDs and DAP, N,Co-CDs were applied to establish ratiometric fluorescent probes for the indirect detection of cholesterol and uric acid that participated in enzyme-catalyzed H_2O_2-generation reactions. The established IFE-based fluorescent probes exhibited relatively low detection limits of 3.6 nM for cholesterol and 3.4 nM for uric acid, respectively. The fluorescent probe was successfully utilized for the determination of cholesterol and uric acid in human blood serum with satisfying results, which provided an informed perspective on the applications of such doped CDs to explore the specific and sensitive nanoprobe in disease diagnoses and clinical therapy.

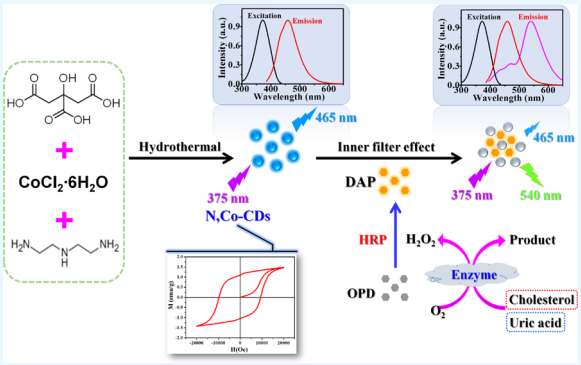

1. INTRODUCTION

As a rising star of functional carbon-based nanomaterial family, carbon dots (CDs) have attracted numerous concerns in biosensing, cell imaging, and nanomedicine due to their unique photochemical properties, good photostability, and superior biocompatibility.[1,2] Due to the facile manipulating feature of heteroatom-doped CDs, metal element-doped CDs become a promising powerful strategy to enhance the photochemical performances and enlarge the potential application capabilities of CDs.[3−6] Recently, some strategies are developed to prepare transition-metal element-doped CDs for different biological applications.[7,8] Yao et al. explored magnetofluorescent CDs for targeted dual-modality cellular imaging and important drug delivery.[9] Jia et al. constructed magnetofluorescent CDs for bimodal cellular imaging and photodynamic therapy.[10] Besides these, magnetic CDs exhibit strong ability in trapping and extracting pathogenic bacteria and cancer cells from complicated sample matrixes, showing potential biological applications in disease diagnosis and cancer therapy.[11,12] Due to the superior biological safety and good magnetic property of Co element, Co element has been widely selected to dope into CDs for obtaining fluorescent and/or magnetic CDs for magnetofluorescent dual-modality bioimaging.[8,13] On the other hand, nonmetal N element is also the frequently used element to efficiently improve the photochemical property of CDs.[14] Although nonmetal N element and metal Co element exhibit the most preferable influences on the optical and magnetic properties of CDs and thus on their biological application performances, synthetic pathways toward fluorescent magnetic N and Co co-doped CDs (N,Co-CDs) are still rare. As far as we know, relative biological application of fluorescent magnetic N,Co-CDs in sensing areas is never reported. It is very necessary to create a cost-efficient and high-output synthesis strategy for producing fine fluorescent

Received: March 29, 2019
Accepted: May 14, 2019
Published: May 28, 2019

DOI: 10.1021/acsomega.9b00874
ACS Omega 2019, 4, 9333−9342

magnetic N,Co-CDs with superior optical-magnetic property and explore their photochemical properties and potential applications in biosensing.

Cholesterol and uric acid are essential and important biomarkers in the clinical diagnosis of several serious diseases correlated with their changes in human blood serum.[15] A higher amount of cholesterol in blood is usually associated with nephrosis and diabetes mellitus and so on, but a lower amount of cholesterol in blood is often related with anemia, hyperthyroidism, Alzheimer's disease and so on.[16,17] Moreover, an extra high amount of uric acid in blood is closely related with metabolic disorders but an extra low amount of uric acid may cause some serious diseases.[18,19] Therefore, monitoring of the cholesterol and uric acid levels in human blood serum is much important for the diagnosis of several serious diseases. Numerous analytical methods were explored for the detection of cholesterol and uric acid in different biological samples, including electroanalysis,[20,21] surface plasmon resonance,[22] chemiluminescence,[23] field effect transistor,[24] and liquid chromatograph.[25] Although these methods can effectively detect cholesterol and uric acid in several samples, the requirement of expensive equipments and complicated sample pretreatments limit their applications for simple and rapid determination. So, the exploration of rapid, economic, sensitive, and effective detection strategies for the detection of cholesterol and uric acid in human blood serum becomes a vital public health objective.

Cholesterol and uric acid can be catalyzed by their specific enzymes to produce H_2O_2, so it is possible to develop efficient strategies for the detection of H_2O_2 that can be used for the indirect quantification of cholesterol and uric acid. More attention has been unremittingly paid to the indirect detection of cholesterol and uric acid through enzyme-catalyzed H_2O_2-generation reactions recently,[16−19] since such strategies can avoid influence from coexisting substances. Ratiometric fluorescence strategy allows the simultaneous measuring of the ratio variations in two well-resolved fluorescent intensities under one excitation wavelength.[26,27] Such ratiometric fluorescence measurement can omit the drawback from single fluorescence measurement efficiently and improve the sensitivity of the fluorescent assay drastically, resulting in the exploitation of the practical applications of carbon-based nanomaterials in biological areas.[28−30] However, nonmetal element and metal element co-doped fluorescent magnetic CDs are rarely utilized as ratiometric fluorescent probes for the detection of cholesterol and uric acid through monitoring H_2O_2 amount. Due to the good photochemical properties of nonmetal element and metal element co-doped fluorescent magnetic CDs, it is valuable and meaningful to establish doped CD-based ratiometric fluorescent probes for specific and sensitive detections of cholesterol and uric acid taking part in enzyme-catalyzed H_2O_2-generation reactions.

Inspired by such a situation, we innovatively designed fluorescent magnetic N,Co-CDs as a ratiometric fluorescent probe for cholesterol and uric acid detections in human blood serum. As shown in Scheme 1, citric acid (CA), cobalt(II) chloride hexahydrate ($CoCl_2{\cdot}6H_2O$), and diethylenetriamine (DETA) were used as precursors for the convenient synthesis of fluorescent magnetic N,Co-CDs through realizable one-pot hydrothermal method for the first time. Because of the co-doping of nonmetal N element and metal Co element, N,Co-CDs possess excellent optical properties and good ferromagnetic property. In the detection process, colorless *o*-phenylenediamine (OPD) can be oxidized by H_2O_2 under the catalysis of horseradish peroxidase (HRP) to produce fluorescent 2,3-diaminophenazine (DAP). Since the absorption spectrum of DAP can partially overlap with the emission spectrum of N,Co-CDs, DAP can quench the fluorescence of N,Co-CDs through the inner filter effect (IFE) mechanism. As a consequence, an ultrasensitive and highly selective ratiometric fluorescence universal platform toward cholesterol and uric acid involved in enzyme-catalyzed H_2O_2-generation reactions was developed. To the best of our knowledge, this is the first but selective and sensitive assay for cholesterol and uric acid determination through the IFE process between fluorescent magnetic N,Co-CDs and DAP, which is identified as a valuable strategy in biomarker-related disease diagnosis and clinical therapy.

Scheme 1. Schematic Illustration of the Preparation of Fluorescent Magnetic N,Co-CDs and Detection Processes of Cholesterol and Uric Acid

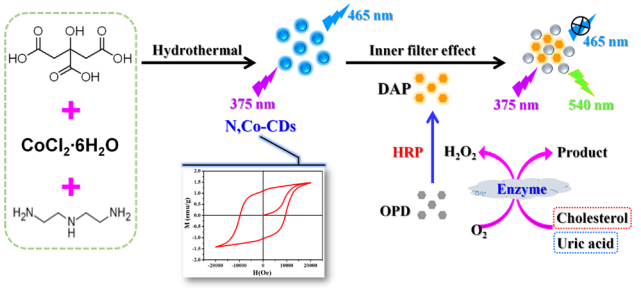

2. RESULTS AND DISCUSSION

2.1. Structure Characterizations of N,Co-CDs. As illustrated in Figure 1a, N,Co-CDs present a primary orbicular shape and spread around evenly without obvious aggregation in transmission electron microscopy (TEM). According to the statistical analysis of around 200 particles, the sizes of N,Co-CDs are in the range from 2.0 to 4.8 nm and the average size is 3.37 nm (insert in Figure 1a), implying the relative smaller size of N,Co-CDs than those of other reported N-CDs.[15,31] These N,Co-CDs possess a clear lattice structure and a discernible lattice spacing of approximately 0.21 nm (insert in Figure 1a), which is highly consistent with the value of the (100) planes of graphitic carbon.[32] As indicated in Figure 1b, the X-ray diffraction (XRD) pattern of N,Co-CDs shows an intense diffraction peak 2θ at 24.5° that is often correlated with the C(002) plane and the poor diffraction peak 2θ at 42.5° is assigned to the C(100) plane, respectively.[33] According to the Bragg equation,[34] the interlayer distance (*d*-spacing value) can be calculated to be 0.36 and 0.21 nm for the diffraction peaks of C(002) plane and C(100) plane, respectively, which matches well with the results obtained from the high-resolution TEM (HRTEM).

The structure and functional groups of N,Co-CDs were continuously characterized by Fourier transform infrared spectroscopy (FT-IR). As indicated in Figure 2a, two intense absorption peaks at 3370 and 3058 cm^{-1} are probably associated with the characteristic stretching vibrations of O−H/N−H and C−H, respectively.[13,15] Three absorption peaks located at 1705, 1647, and 1558 cm^{-1} are associated with the stretching vibrations of C═O, multiple ═C−H, and C═C bonds, respectively.[6,15] Two absorption peaks located at 1428 and 1246 cm^{-1} are ascribed to the stretching vibrations of C−

DOI: 10.1021/acsomega.9b00874
ACS Omega 2019, 4, 9333−9342

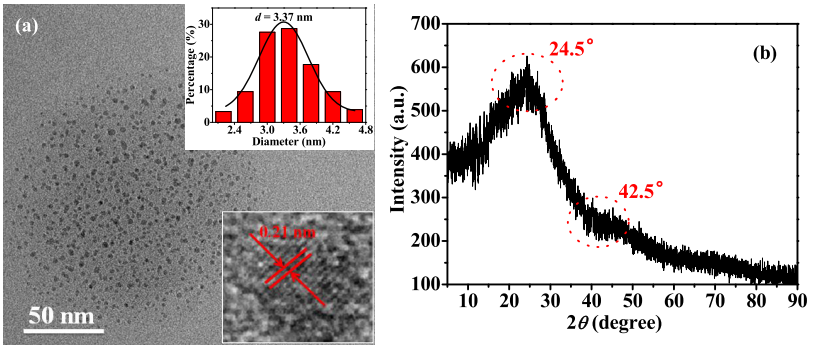

Figure 1. (a) TEM image of N,Co-CDs. Insert: HRTEM image and particle size distribution curve of N,Co-CDs. (b) XRD pattern of N,Co-CDs.

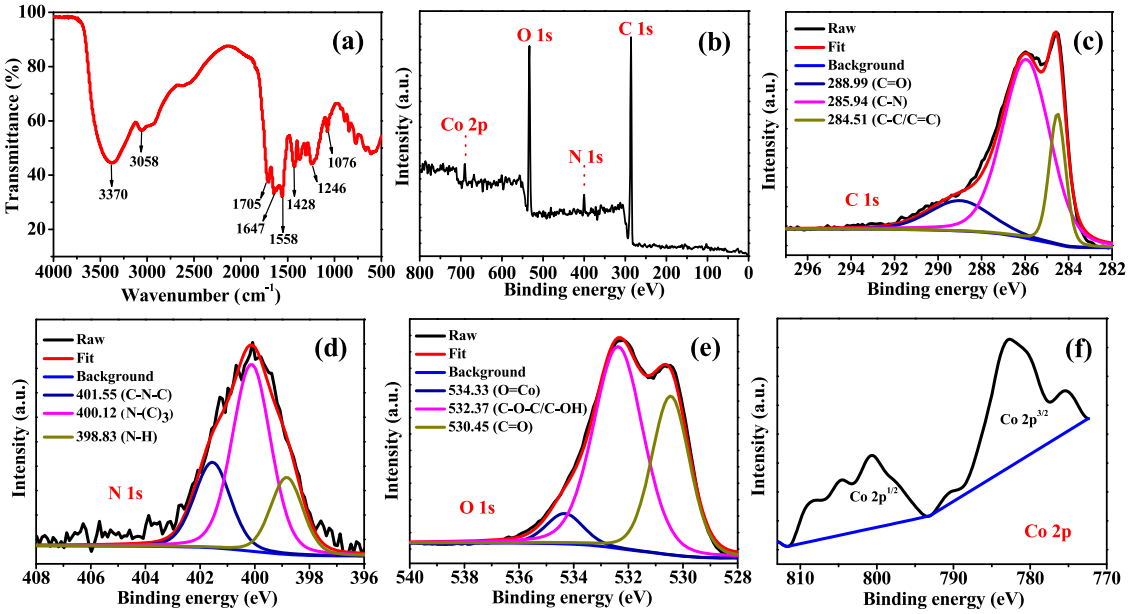

Figure 2. (a) FT-IR spectrum of N,Co-CDs. (b) X-ray photoelectron spectroscopy (XPS) survey spectrum, (c) C 1s XPS spectrum, (d) N 1s XPS spectrum, (e) O 1s XPS spectrum, and (f) Co 2p XPS spectrum of N,Co-CDs.

N and C−O bonds, respectively.[15] The absorption peak at 1033 cm^{-1} is ascribed to the stretching vibration of C−O−C bond.[35] All of these results imply the existences of multiple oxygenated and nitrous functional groups in N,Co-CDs, suggesting their biological applications in targeted drug delivery during clinical therapy.

Detailed surface composition and elemental contents of N,Co-CDs were investigated by X-ray photoelectron spectroscopy (XPS). As shown in Figure 2b, the XPS survey spectrum of N,Co-CDs clearly exhibits characteristic peaks of C 1s at 284.9 eV, N 1s at 400.0 eV, O 1s at 531.8 eV, and Co 2p at 782.5 eV, respectively. High-resolution XPS spectrum of C 1s is divided into three contributions (Figure 2c), including C═C/C−C at 284.51 eV, C−N at 285.94 eV, and C═O at 288.99 eV, respectively.[32,36] High-resolution XPS spectrum of N 1s shows three contributions at 401.55, 400.12, and 398.83 eV (Figure 2d), which are attributed to C−N−C, N−$(C)_3$, and N−H, respectively.[31] High-resolution XPS spectrum of O 1s shows three contributions at 534.33, 532.37, and 530.45 eV (Figure 2e), ascribing to Co═O, C−O−C/C−OH, and C═O, respectively.[13] From the high-resolution XPS spectrum of Co 2p (Figure 2f), Co $2p_{3/2}$ at 782.80 eV and Co $2p_{1/2}$ at 800.60 eV are assigned to its spin−orbit splitting[13] and the binding energies of 790.60 and 804.50 eV are ascribed to their shake-up resonance transitions, respectively. All of these results provide a strong evidence of the existence of Co^{2+} ions in the obtained N,Co-CDs backbone.[13] According to the result of the elemental analysis, N,Co-CDs are composed of C 38.90 wt %, H 7.63 wt %, N 18.94 wt %, Co 8.06 wt %, and O (calculated) 26.47 wt % (Table S1a) and the empirical formula of N,Co-CDs is approximately $C_{25}H_{56}N_{10}CoO_{12}$ (Table S1b). All of these results reconfirm not only the successful doping of N and Co elements in N,Co-CDs but also the existences of multiple oxygenated and nitrous functional groups in these N,Co-CDs.

2.2. Optical and Magnetic Properties of N,Co-CDs. As shown in Figure 3a, N,Co-CDs show an evident UV−vis absorption peak at 240 nm corresponding to the $\pi \rightarrow \pi^*$ electronic transition of aromatic sp^2 carbon.[15] The typical absorption peak at 357 nm is assigned to the $n \rightarrow \pi^*$ electronic transitions of C═O, C═N, and other bonds in N,Co-CDs, resulting in these N,Co-CDs emitting strong blue fluorescence under a handheld UV lamp with 365 nm wavelength (insert in Figure 3a).[37−39] These N,Co-CDs emit blue fluorescence according to the Commission International d'Eclairage (CIE) 1931 2° chromaticity diagram (Figure S1).[40] As further shown in Figure 3b,c, the emission wavelength of N,Co-CDs red-shifts from 435 to 475 nm with the excitation wavelength increasing from 320 to 420 nm, suggesting the emission

DOI: 10.1021/acsomega.9b00874
ACS Omega 2019, 4, 9333−9342

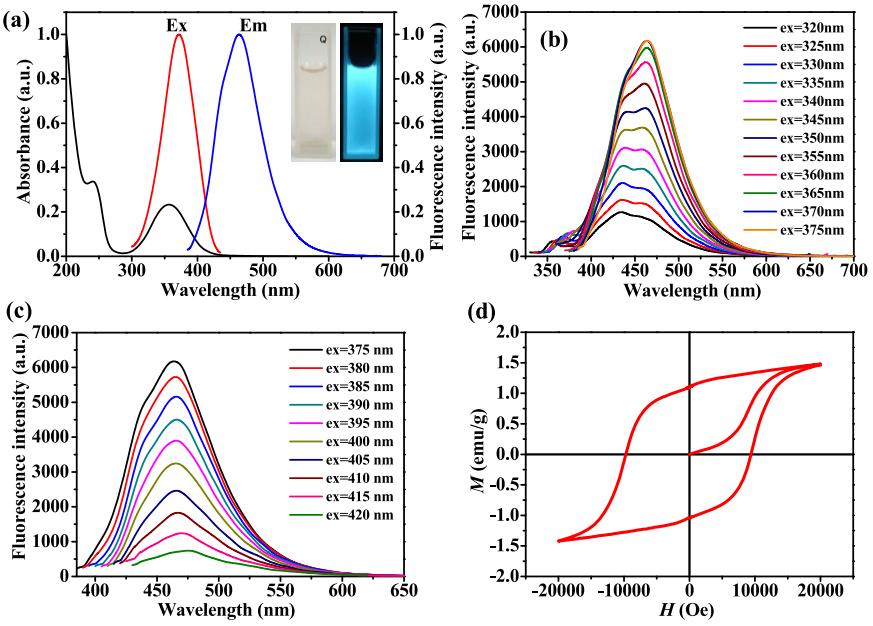

Figure 3. (a) UV−vis absorption spectrum and excitation spectrum (λ_{em} = 465 nm) and emission spectrum (λ_{ex} = 375 nm) of N,Co-CDs. Insert: Photograph of N,Co-CDs under the excitation of white light (left) and UV lamp with a 365 nm (right) wavelength. (b, c) Fluorescence spectra of N,Co-CDs with the excitation wavelength increasing from 320 to 420 nm. (d) $M-H$ behavior of N,Co-CDs.

wavelength-dependent feature of these N,Co-CDs.[41] The maximum excitation wavelength and emission wavelength of N,Co-CDs are 375 and 465 nm, respectively. By using the integrating sphere, the absolute fluorescent quantum yield of N,Co-CDs appearing at 465 nm upon a 375 nm excitation is calculated to be 71.91%, which is much higher than that of some reported doped CDs.[13,15]

The time-resolved fluorescence spectrum of N,Co-CDs was recorded, and the fluorescent lifetime of N,Co-CDs was measured according to time-correlated single-photo counting system. The fluorescent decay traces are well-fitted by the following double-exponential equation

$$\langle \tau \rangle = \left(\sum b_i \tau_i^2\right) / \left(\sum b_i \tau_i\right) \quad (1)$$

Herein, τ_i is the fluorescent lifetime of N,Co-CDs and b_i is the normalized pre-exponential factor, respectively. It is clearly shown in the insert table of Figure S2 that N,Co-CDs exhibit two fluorescence decay components: τ_1 (b_i) of 7.39 ns (17.83%) and τ_2 (b_2) of 13.76 ns (82.17%), respectively. The average fluorescent lifetime of N,Co-CDs is about 13.10 ns (excited at 340 nm) (insert table of Figure S2) that is much longer than that of some reported doped CDs.[13,15,42] As further presented in Figures S3−S5, the fluorescence intensity of N,Co-CDs remains unchanged obviously under long time UV light irradiation (180 min) or in buffer solution with a wide pH value (3.0−11.0) and extremely high NaCl concentration (3.0 M). The fluorescence of N,Co-CDs remains almost constant even after 1 month storage at room temperature. The excellent photochemical stability of N,Co-CDs under extremely harsh environment conditions and long time storage promotes their further application in biological analysis and live cell imaging.

Due to the doping of Co element, the as-prepared N,Co-CDs may possess magnetic property.[8] The magnetic property of N,Co-CDs was measured at room temperature, and the field-dependent magnetization ($M-H$) curve is shown in Figure 3d. The magnetic hysteresis loop in the $M-H$ curve of N,Co-CDs shows that the these N,Co-CDs exhibit a ferromagnetic behavior with a saturated magnetization (M_s) value of 1.476 emu/g and a coercive force (H_c) of 9.68×10^3 Oe. Compared with other transition-metal ion-doped CDs and some hybrid CD nanoconstucts,[8,11,12] the M_s value of N,Co-CDs is much smaller, implying the relatively low magnetic property of these N,Co-CDs. The ferromagnetism behavior of N,Co-CDs is only attributed to the unpaired electrons and the magnetization of the doped Co element. The extra low content of Co (8.06 wt %) in these N,Co-CDs may result in the weak ferromagnetic behavior of N,Co-CDs. Meanwhile, the spin canting effect in Co atom surface results in the reduced magnetization of N,Co-CDs. For these N,Co-CDs with smaller sizes, the magnetization is inclined to decrease at room temperature after long time storage. Although numerous paramagnetic and super-paramagnetic CDs are suitable for the magnetic resonance imaging, the ferromagnetic property of N,Co-CDs makes them potentially applicable for trapping and extracting pathogenic bacteria and cancer cells in complicated sample matrixes.

Cyclic voltammograms (CVs) were recorded to calculate the highest occupied molecular orbital (HOMO) and the lowest unoccupied molecular orbital (LUMO) energy levels of N,Co-CDs and N-CDs. CVs were carried out in tetrabutylammonium hexafluorophosphate solution by using the standard three-electrode system: working electrode of CDs or N,Co-CDs coated glassy carbon electrode, counter electrode of platinum wire electrode, and reference electrode of Ag/AgCl electrode, respectively.[43] HOMO and LUMO energy levels in electronvolt as well as the electrochemical energy gap (E_g in electronvolt) of these CDs can be calculated according to the following equations[43,44]

$$E_{(HOMO)} = -e(E_{ox} + 4.4)\ (eV) \text{ and } E_{(LUMO)} = -e(E_{red} + 4.4)\ (eV) \quad (2)$$

DOI: 10.1021/acsomega.9b00874
ACS Omega 2019, 4, 9333−9342

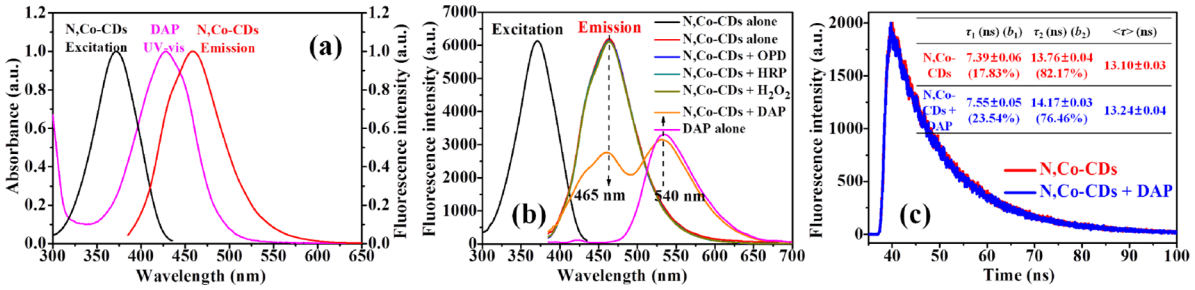

Figure 4. (a) UV−vis absorption spectrum of DAP; excitation and emission spectra of N,Co-CDs. (b) Excitation spectrum of N,Co-CDs alone and emission spectra of N,Co-CDs alone (100 μg/mL), N,Co-CDs + OPD (5 mM), N,Co-CDs + HRP (10 μg/mL), N,Co-CDs + H_2O_2 (500 μM), N,Co-CDs + DAP (100 μM), and DAP alone (100 μM). (c) Fluorescence decay traces of N,Co-CDs before and after the addition of DAP. The test was made at the emission wavelength of 465 nm. τ is the fluorescent lifetime of N,Co-CDs, and b is the normalized pre-exponential factor.

Herein, E_{ox} and E_{red} represent the oxidation and reduction potentials, respectively. It is clear from Figure S6 that the E_{red} values are determined to be −0.4064 V for N,Co-CDs and −0.4027 V for N-CDs, respectively. Therefore, the LUMO energy levels are around −3.99 eV for N,Co-CDs and −4.00 eV for N-CDs. Due to the irreversible oxidation behavior, the HOMO energy levels can be calculated indirectly by the following equations[44]

$$E_{(HOMO)} = E_{(LUMO)} - E_g \text{ (eV)} \quad (3)$$

The optical energy band gap (E_g) is the absorption edge of the absorption peak (357 nm) of CDs in the UV−vis spectrum, and E_g is estimated to be 3.61 eV. So, the HOMO energy levels are −7.60 eV for N,Co-CDs and −7.61 eV for N-CDs. As shown in Figure S7, both the HOMO and the LUMO energy levels of N-CDs are approximately equal to those of N,Co-CDs; thus, the spectral properties of CDs remain almost unchanged before or after the doping of metal Co element (Figures S8 and S9).

2.3. Fluorescence Detection Mechanism. In this assay, a novel fluorescent magnetic N,Co-CD-based ratiometric fluorescent probe for the detection of cholesterol and uric acid, which responded to enzyme-catalyzed H_2O_2-generation reaction, was developed. As shown in Scheme 1, CA, $CoCl_2 \cdot 6H_2O$, and DETA are used to prepare N,Co-CDs with emission wavelength of 465 nm by one-pot hydrothermal method. H_2O_2, which is the product in the oxidation reactions of cholesterol and uric acid with O_2 under the catalysis of their specific oxidoreductases (cholesterol oxidase and urate oxidase), can oxidize OPD to produce DAP with the catalysis of HRP. DAP with emission wavelength of 540 nm can quench the fluorescence of several carbon-based fluorescence nanomaterials through IFE.[15,29] Therefore, such N,Co-CDs with excellent properties can be used as the powerful ratiometric fluorescent probes for indirect detection of cholesterol and uric acid.

The possible fluorescence quenching mechanism in N,Co-CDs/DAP system may be probably IFE.[45] As seen in Figure 4a, DAP shows a strong UV−vis absorption peak located at 430 nm and the absorption spectrum of DAP can partially overlay with the emission spectrum of N,Co-CDs. Our preliminary results showed that the molar absorption coefficients of DAP at 375 and 465 nm were about 6.36 × 10^3 L/(mol cm) and 9.01 × 10^3 L/(mol cm) whereas OPD exhibits almost no absorbance at both 375 and 465 nm. These results suggest the strong absorption ability of DAP and the weak absorption ability of OPD at these two wavelengths. As a consequence, DAP with strong UV−vis absorption ability can absorb both the excitation light and the emission light of N,Co-CDs whereas OPD may not affect the emission light of N,Co-CDs at all. As indicated in Figures 4b andS10, N,Co-CDs show metal ion, amino acid, and carbohydrate insensitivity. Obviously, other materials (OPD and HRP) during the enzyme-catalyzed DAP-generation reaction exhibit no influences on the fluorescence of N,Co-CDs. Thus, these N,Co-CDs are efficient fluorescence donor agents in N,Co-CDs/DAP system based on IFE.

To further understand the detailed fluorescence quenching mechanism of N,Co-CDs/DAP system, the fluorescent lifetimes of N,Co-CDs without DAP were recorded and the results were displayed in Figure 4c. As exhibited in the insert table of Figure 4c, the corresponding average fluorescent lifetime of N,Co-CDs with DAP is about 13.24 ns. The fluorescent lifetime of N,Co-CDs remains almost constant, illustrating that there is no significant electron or energy transfer process in N,Co-CDs/DAP system.[46] The ζ potentials of N,Co-CDs, DAP, and N,Co-CDs/DAP system are all positive (Figure S11), so the nonignorable electrostatic repulsive force between N,Co-CDs and DAP exists. The distance between N,Co-CDs and DAP is hardly shorter than 10 nm; thus, the Förster resonance energy transfer (FRET) cannot occur in this system.[47] All results suggest that the fluorescence quenching mechanism in N,Co-CDs/DAP system is attributed to IFE rather than photoinduced electron transfer or Förster resonance energy transfer (FRET).

2.4. Fluorescence Detection of Cholesterol and Uric Acid. These fluorescent magnetic N,Co-CDs are used as fluorescent nanoprobes for the indirect determinations of cholesterol and uric acid through enzyme-catalyzed H_2O_2-generation reaction. Before detection, several important analytical parameters need to be optimized previously: (a) amount of N,Co-CDs, (b) concentration of OPD, (c) amount of HRP, (d) pH value of phosphate buffer (3.15 mM Na_2HPO_4 and 6.85 mM NaH_2PO_4), (e) incubation temperature, (f) reaction time, (g) amount of cholesterol oxidase, and (h) amount of urate oxidase. Fluorescence intensity of N,Co-CDs at 465 nm (I_{465}) and that of DAP at 540 nm (I_{540}) were recorded. According to the ratiometric fluorescence signal I_{540}/I_{465} shown in Figures S12−S14, the following optimal analytical parameters are found to obtain the best result: (a) 100 μg/mL N,Co-CDs, (b) 5 mM OPD, (c) 10 μg/mL HRP, (d) pH 6.5 of phosphate buffer, (e) incubation temperature of 37 °C, (f) reaction time of 25 min, (g) 0.05 U/mL cholesterol oxidase, and (h) 0.06 U/mL urate oxidase.

DOI: 10.1021/acsomega.9b00874
ACS Omega 2019, 4, 9333−9342

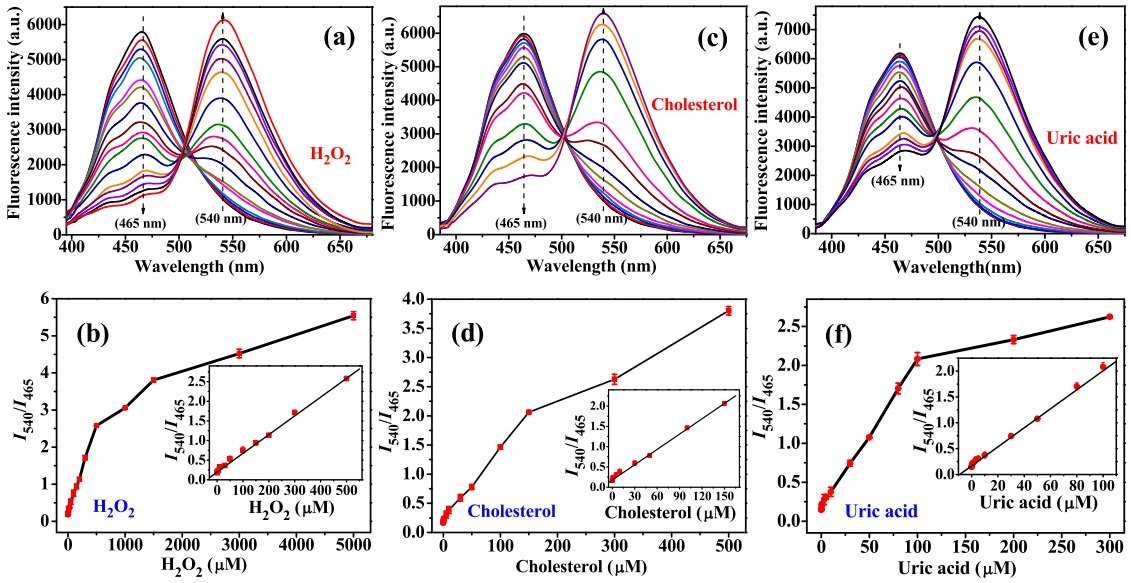

Figure 5. Fluorescence spectra of this ratiometric fluorescent probe with increasing concentrations of H_2O_2 (a), cholesterol (c), and uric acid (e). (b) The curve of I_{540}/I_{465} value versus the H_2O_2 concentration in the range 0.01−5000 μM; insert: calibration curve of H_2O_2 detection in the range 0.01−500 μM. (d) The curve of I_{540}/I_{465} value versus the cholesterol concentration in the range 0.01−500 μM. Insert: Calibration curve of cholesterol detection in the range 0.01−150 μM. (f) The curve of I_{540}/I_{465} value versus the uric acid concentration in the range 0.01−300 μM. Insert: calibration curve of uric acid detection in the range 0.01−100 μM.

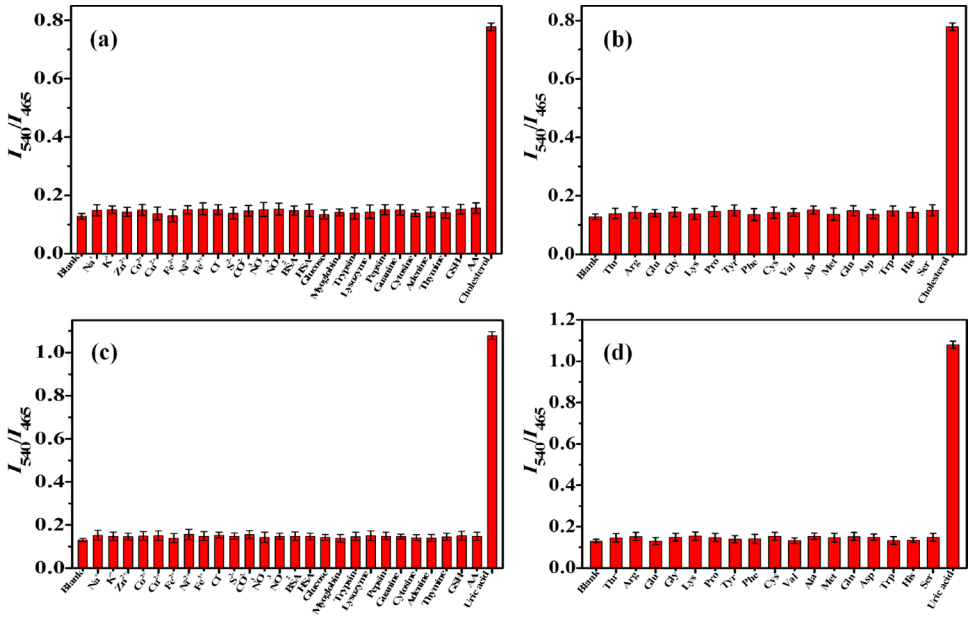

Figure 6. Ratiometric fluorescence signal I_{540}/I_{465} with various concentrations of different interferences for the detections of cholesterol (a, b) and uric acid (c, d). The concentrations of cholesterol and uric acid were 50 μM, and the concentrations of other interferences were all 100 μM.

Under the optimized analytical parameters (Figure S12), the fluorescence spectra of the sensing platform were measured in the presence of H_2O_2 with the concentration range of 0.01 μM to 5 mM. As shown in Figure 5a, the I_{465} value decreases gradually whereas the I_{540} value increases correspondingly with the increasing concentration of H_2O_2 and the ratiometric fluorescence signal I_{540}/I_{465} increases accordingly (Figure 5b). As indicated in the insert of Figure 5b, when the concentration of H_2O_2 increases from 0.01 to 500 μM, a good linear relationship exists between the I_{540}/I_{465} value and the concentration of H_2O_2 with the linear equation I_{540}/I_{465} = 0.00477[H_2O_2] (μM) + 0.1973 (n = 3, correlation coefficient of 0.9982). The detection limit (LOD) of H_2O_2 is calculated to be 6.9 nM based on $3\sigma/K$ (σ is the standard deviation of blank measurement, and K is the slope of the calibration graph), which is better than some existing fluorescence probes for H_2O_2.[15,30] Such a fluorescent magnetic N,Co-CD-based ratiometric fluorescent probe exhibits ultrasensitive detection of H_2O_2, implying that this method can be used to detect cholesterol and uric acid indirectly.

2.4.1. Sensitivity of Cholesterol and Uric Acid Detection. This fluorescent magnetic N,Co-CD-based ratiometric fluorescence sensing platform was used for the detection of cholesterol. Under the optimized conditions (Figures S12 and

DOI: 10.1021/acsomega.9b00874
ACS Omega 2019, 4, 9333−9342

S13), the fluorescence spectra of this sensing platform were recorded after adding increasing concentration of cholesterol from 0.01 to 500 μM. It is shown that the I_{465} value decreases whereas the I_{540} value increases gradually with the increasing concentration of cholesterol (Figure 5c). The ratiometric fluorescence signal I_{540}/I_{465} increases according to the increment of the concentration of cholesterol (Figure 5d). As further shown in the insert of Figure 5d, the ratiometric fluorescence signal I_{540}/I_{465} exhibits a good linear relationship to the cholesterol concentration in the range 0.01−150 μM. The linear fitting equation is I_{540}/I_{465} = 0.01258[cholesterol] (μM) + 0.1767 (n = 3, correlation coefficient of 0.9975), and the LOD of cholesterol is 3.6 nM based on $3\sigma/K$.

This fluorescent magnetic N,Co-CD-based ratiometric fluorescent sensing platform was continuously used to detect uric acid. Under optimized conditions (Figures S12 and S14), the fluorescence spectra of this sensing platform were recorded after the addition of increasing concentration of uric acid from 0.01 to 300 μM. It is obvious that the I_{465} value decreases whereas the I_{540} value increases gradually with the increasing concentration of uric acid (Figure 5e). As shown in Figure 5f, the ratiometric fluorescence signal I_{540}/I_{465} increases with the increment of the concentration of uric acid. Furthermore, the ratiometric fluorescence signal I_{540}/I_{465} shows a linear relationship with the uric acid concentration in the range of 0.01−100 μM (insert of Figure 5f). The fitted linear equation is I_{540}/I_{465} = 0.01838[uric acid] (μM) + 0.1672 (n = 3, correlation coefficient of 0.9984), and the LOD of uric acid is 3.4 nM based on $3\sigma/K$.

Comparing with other reported colorimetry, fluorescence spectrometry, chemiluminescence, and electrochemical methods by using other nanomaterials, our method exhibits ultrawider linear ranges and relatively lower detection limits for the detections of cholesterol and uric acid. As shown in Tables S2 and S3, such N,Co-CD-based ratiometric fluorescence sensing platform shows comparable or even superior sensitivity for the determination of cholesterol and uric acid. Most importantly, these fluorescent magnetic N,Co-CDs possessing magnetic property are expediently separated from the detection system by using the magnet, which makes them reusable during this detection strategy.

2.4.2. Selectivity and Practicability Investigations. To investigate the selectivity of this ratiometric fluorescence universal platform for the detection of cholesterol and uric acid, the interferences of common ions, amino acids, carbohydrates, nucleotides, and proteins on the ratiometric fluorescence signal I_{540}/I_{465} were studied. As shown in Figure 6, when the concentrations of cholesterol and uric acid are 50 μM whereas all of the concentrations of other interferences are 100 μM, these interferences have no significant influences on the ratiometric fluorescence measurement. Although these N,Co-CDs are sensitive toward Ag^+ and Fe^{3+} (Figure S10), the interference of Ag^+ on the detection system can be omitted due to the generation of Ag_3PO_4 precipitate in the phosphate buffer. This sensing platform is also insensitive toward Fe^{3+}, which ascribes to the negligible background signal of such a ratiometric fluorescence strategy by using the ratiometric fluorescence signal I_{540}/I_{465} as the detection signal.

Due to the ultrahigh specificity of the enzyme−substance reactions, the as-prepared sensing strategy exhibits excellent selectivity for cholesterol and uric acid determinations. In the proposed sensing method, enzyme-catalyzed H_2O_2-generation reaction is the most important section for detection of signal transformation. But in real human blood serum samples, the endogenous substances (ascorbic acid, L-cysteine, and glutathione) can reduce and consume the produced H_2O_2 to affect the detection results, which is vital to the whole strategy. However, when these endogenous substances coexist in cholesterol and uric acid, the ratiometric fluorescence signal I_{540}/I_{465} remains almost constant (Figure S15). Since the amounts of ascorbic acid, L-cysteine, and glutathione in real human blood serum samples are much lower than those of cholesterol and uric acid, the influences of these interferences can be omitted. These results confirm the good specificity and the potential biological application of this ratiometric fluorescence sensing approach for cholesterol and uric acid in real human blood serum samples.

The practicability of this ratiometric fluorescence universal platform was investigated through detecting cholesterol and uric acid in human blood serum by using the standard addition approach. As shown in Table S4, the amounts of cholesterol found in these human blood serum are in accordance with the reported values (2.86−5.98 mM).[48] As indicated in Table S5, the amounts of uric acid found in human blood serum are in accordance with the reported values (0.12−0.46 mM).[19] The recoveries for cholesterol with three different concentrations (5, 50, and 100 μM) in human serum samples increase from 95.8 to 103.6%, and the relative standard deviations are all lower than 1.3% for three replicate measurements. The recoveries for uric acid with three different concentrations (0.5, 5, and 50 μM) in human serum samples increase from 98.6 to 103.7%, and the relative standard deviations are all lower than 1.1% for three replicate measurements. Therefore, this strategy is a promising design for the detections of cholesterol and uric acid in real samples. All of the results prove the good selectivity and the super practicability of such N,Co-CD-based fluorescent probes for biomarker detections in real biological samples.

3. CONCLUSIONS

In summary, N,Co-CDs were prepared through a simple and convenient one-pot hydrothermal technique by using CA, $CoCl_2{\cdot}6H_2O$, and DETA as precursors. Due to the co-doping of nonmetal N element and metal Co element, N,Co-CDs showed excellent photochemical properties and ferromagnetic property. On the basis of the IFE process in N,Co-CDs/DAP system, a N,Co-CDs-based ratiometric fluorescent probe was established for the determination of cholesterol and uric acid indirectly. The detection limits of cholesterol and uric acid were 3.6 and 3.4 nM, respectively, which met the requirements for the highly sensitive monitoring of low levels of cholesterol and uric acid in human blood serum. The proposed N,Co-CD-based probing platform is a desirable approach for biomarker monitoring in disease diagnosis and clinical therapy.

4. EXPERIMENTAL SECTION

4.1. Reagents and Materials. CA, $CoCl_2{\cdot}6H_2O$, DETA, OPD, HRP, uric acid, cholesterol, and cholesterol esterase were obtained from Aladdin Chemical Co., Ltd. (Shanghai, China). DAP, cholesterol oxidase, urate oxidase, amino acids, and all other biological substances were obtained from Sigma-Aldrich Co., Ltd. (St. Louis, MO). All chemical reagents were purchased from Sinopharm Chemical Reagent Co., Ltd. (Shanghai, China). All reagents were of the highest commercially available purity and used directly as received.

DOI: 10.1021/acsomega.9b00874
ACS Omega 2019, 4, 9333−9342

Ultrapure water with resistivity of 18.2 MΩ cm was prepared through Millipore-Q Academic purification system (Bedford).

4.2. Synthesis of N,Co-CDs, and N-CDs. The fluorescent property of N,Co-CDs can be affected by the amount of CA, the volume of DETA, the amount of $CoCl_2·6H_2O$, the reaction temperature, and the reaction time. As shown in Figure S16, the optimal conditions for synthesis of N,Co-CDs were as follows: 2.0 g of CA, 0.07 mL of DETA, 0.4 g of $CoCl_2·6H_2O$, 160 °C, and 8 h. Therefore, for the synthesis of N,Co-CDs, 2.0 g of CA and 0.4 g of $CoCl_2·6H_2O$ were first dissolved in 20 mL of ultrapure water and then 0.07 mL of DETA was added into the above solution. The solution was dissolved completely by an ultrasonic method for 10 min. Thereafter, the solution was transferred into a 50 mL Teflon-lined stainless steel autoclave chamber and reacted at 160 °C for 8 h. After natural cooling to room temperature, the solution was collected and dialyzed in a dialysis bag with a cutoff molecular weight of 500 Da for 72 h. Finally, the outside solution was collected and concentrated to be about 100 mL under rotary evaporation. The solid powder of N,Co-CDs was finally obtained via vacuum freeze-drying for 48 h. This N,Co-CD powder was stored at 4 °C for further applications. The synthesis and purification processes of N-CDs are all same as above just without the addition of $CoCl_2·6H_2O$.

4.3. Characterizations of N,Co-CDs and N-CDs. TEM and HRTEM images were taken with a JEM-2100F high-resolution transmission emission microscope (JEOL, Japan). XRD spectrum was measured on a Bruker D-8 Advance Powder X-ray diffractometer (Bruker, Germany). XPS spectra were taken with ESCALAB 250Xi X-ray photoelectron spectroscopy (Thermo Fisher Scientific). FT-IR spectrum was recorded on a Thermo Nicolet iS10 spectrometer (Thermo Fisher Scientific). Elemental analysis was carried out on a Vario EL/Micro Cube organic element analyzer (Elementar Analysensysteme GmbH, Germany). Magnetic property was recorded by using a VersaLab Vibration Sample Magnetometer (Quantum Design). UV−vis absorption spectra were recorded on a Shimadzu UV-3600 Plus UV−vis−NIR spectrophotometer (Shimadzu, Japan). Fluorescence spectra were recorded on a Thermo Scientific Lumina fluorescence spectrometer (Thermo Fisher Scientific). Time-resolved fluorescence spectra were measured on a Horiba Scientific QM-8075 high sensitivity steady-state transient fluorescence spectrometer (HORIBA, Japan). ζ-Potential was recorded on a Zetasizer Nano ZS (Malvern, U.K.). CV curves were obtained from a Chenhua CHI-760E electrochemical workstation (Shanghai, China). The pH values were mediated using a Sartorius PB-10 pH meter (Sartorius, China).

4.4. Fluorescent Sensing of Cholesterol and Uric Acid. For H_2O_2 detection, 500 μL of 30 mM OPD, 30 μL of 1 mg/mL HRP, and 70 μL of different concentrations of H_2O_2 were mixed in 10 mM phosphate buffer (pH = 6.5). The solution was stored in the dark and incubated at 37 °C for 25 min. Then, 100 μL of N,Co-CD solution (3 mg/mL) was added into the mixture and the solution was finally diluted to 3 mL with 10 mM phosphate buffer (pH = 6.5). After additional incubation at 25 °C for 1 min, the fluorescence spectra were recorded under the excitation wavelength of 375 nm and the ratiometric fluorescence signal I_{540}/I_{465} was used to detect H_2O_2.

For the fluorescent sensing of cholesterol and uric acid, 500 μL of 30 mM OPD, 30 μL of 1 mg/mL HRP, 100 μL of different concentrations of cholesterol or uric acid, and 50 μL of 3 U/mL cholesterol oxidase for cholesterol or 60 μL of 3 U/mL urate oxidase for uric acid were mixed thoroughly in 10 mM phosphate buffer (pH = 6.5). The solution was stored in the dark and incubated at 37 °C for 25 min. Then, 100 μL of N,Co-CD solution (3 mg/mL) was added into the mixture. The solution was finally diluted to 3 mL with 10 mM phosphate buffer (pH = 6.5). After additional incubation at 25 °C for 1 min, the fluorescence spectra were recorded under the excitation wavelength of 375 nm. The ratiometric fluorescence signal I_{540}/I_{465} was utilized for the determination of cholesterol and uric acid.

For cholesterol detection in human blood serum, 500 μL of a human blood serum sample was mixed with 10 μL of 1 mg/mL cholesterol esterase to hydrolyze cholesterol ester to produce free cholesterol and then diluted by 100 times by adding 10 mM phosphate buffer (pH = 6.5). For uric acid detection in human blood serum, the human blood serum sample was diluted by 100 times by adding 10 mM phosphate buffer (pH = 6.5). The diluted human blood serum replaced with standard samples was measured as described above.

■ ASSOCIATED CONTENT

Supporting Information

The Supporting Information is available free of charge on the ACS Publications website at DOI: 10.1021/acsomega.9b00874.

CIE color profile; fluorescence decay trace; effects of irradiation time; pH value, and ionic strength on fluorescence; CV curves, energy levels; UV−vis and fluorescence spectra; influences of interferences; ζ-potential data; influences of parameters for detection; influences of parameters for synthesis; elemental analysis; comparison tables; and real sample detection (PDF)

■ AUTHOR INFORMATION

Corresponding Author

*E-mail: qi.xiao@whu.edu.cn. Tel/Fax: +86 771 3908065.

ORCID

Shan Huang: 0000-0002-6133-1853

Yue Zhang: 0000-0002-6140-3757

Notes

The authors declare no competing financial interest.

■ ACKNOWLEDGMENTS

This work was financially supported by the National Natural Science Foundation of China (21864006, 21763005, and 21563006), Natural Science Foundation of Guangxi Province (2017GXNSFDA198034, 2017GXNSFFA198005, and 2016GXNSFBA380118), Guangxi Scientific and Technological Development Projects (AD17195081), China Scholarship Council Project (201708455047), the High-Level-Innovation Team (guijiaoren[2017]38) and Outstanding Scholar Project of Guangxi Higher Education Institutes, and BAGUI Scholar Program of Guangxi Province of China.

■ REFERENCES

(1) Yan, F. Y.; Jiang, Y. X.; Sun, X. D.; Bai, Z. J.; Zhang, Y.; Zhou, X. G. Surface modification and chemical functionalization of carbon dots: A review. *Microchim. Acta* **2018**, *185*, 424.

(2) Wang, H.; Chen, Q. W.; Zhou, S. Q. Carbon-based hybrid nanogels: A synergistic nanoplatform for combined biosensing,

DOI: 10.1021/acsomega.9b00874
ACS Omega 2019, 4, 9333−9342

bioimaging, and responsive drug delivery. *Chem. Soc. Rev.* **2018**, *47*, 4198−4232.
(3) Xu, Q.; Kuang, T. R.; Liu, Y.; Cai, L. L.; Peng, X. F.; Sreeprasad, T. S.; Zhao, P.; Yu, Z. Q.; Li, N. Heteroatom-doped carbon dots: Synthesis, characterization, properties, photoluminescence mechanism and biological applications. *J. Mater. Chem. B* **2016**, *4*, 7204−7219.
(4) Xu, Q.; Liu, Y.; Su, R. G.; Cai, L. L.; Li, B. F.; Zhang, Y. Y.; Zhang, L. Z.; Wang, Y. J.; Wang, Y.; Li, N.; Gong, X.; Gu, Z. P.; Sreeprasad, T. S.; et al. Highly fluorescent Zn-doped carbon dots as Fenton reaction-based bio-sensors: an integrative experimental−theoretical consideration. *Nanoscale* **2016**, *8*, 17919−17927.
(5) Meng, A.; Xu, Q. H.; Zhao, K.; Li, Z. J.; Liang, J.; Li, Q. D. A highly selective and sensitive "on-off-on" fluorescent probe for detecting Hg(II) based on Au/N-doped carbon quantum dots. *Sens. Actuators, B* **2018**, *255*, 657−665.
(6) Bera, K.; Sau, A.; Mondal, P.; Mukherjee, R.; Mookherjee, D.; Metya, A.; Kundu, A. K.; Mandal, D.; Satpati, B.; Chakrabarti, O.; Basu, S. Metamorphosis of ruthenium-doped carbon dots: In search of the origin of photoluminescence and beyond. *Chem. Mater.* **2016**, *28*, 7404−7413.
(7) Xu, Q.; Su, R. G.; Chen, Y. S.; Sreenivasan, S. T.; Li, N.; Zheng, X. S.; Zhu, J. F.; Pan, H. B.; Li, W. J.; Xu, C. M.; Xia, Z. H.; Dai, L. M. Metal charge transfer doped carbon dots with reversibly switchable, ultra-high quantum yield potoluminescence. *ACS Appl. Nano Mater.* **2018**, *1*, 1886−1893.
(8) Pakkath, S. A. R.; Chetty, S. S.; Selvarasu, P.; Murugan, A. V.; Kumar, Y.; Periyasamy, L.; Santhakumar, M.; Sadras, S. R.; Santhakumar, K. Transition metal ion (Mn^{2+}, Fe^{2+}, Co^{2+}, and Ni^{2+})-doped carbon dots synthesized via microwave-assisted pyrolysis: A potential nanoprobe for magneto-fluorescent dual-modality bioimaging. *ACS Biomater. Sci. Eng.* **2018**, *4*, 2582−2596.
(9) Yao, Y. Y.; Gedda, G.; Girma, W. M.; Yen, C. L.; Ling, Y. C.; Chang, J. Y. Magnetofluorescent carbon dots derived from crab shell for targeted dual-modality bioimaging and drug delivery. *ACS Appl. Mater. Interfaces* **2017**, *9*, 13887−13899.
(10) Jia, Q.; Ge, J. C.; Liu, W. M.; Zheng, X. L.; Chen, S. Q.; Wen, Y. M.; Zhang, H. Y.; Wang, P. F. A Magnetofluorescent carbon dot assembly as an acidic H_2O_2-driven oxygenerator to regulate tumor hypoxia for simultaneous bimodal imaging and enhanced photodynamic therapy. *Adv. Mater.* **2018**, *30*, No. e1706090.
(11) Das, R. K.; Pramanik, A.; Majhi, M.; Mohapatra, S. Magnetic mesoporous silica gated with doped carbon dot for site-specific drug delivery, fluorescence, and MR imaging. *Langmuir* **2018**, *34*, 5253−5262.
(12) Nimi, N.; Saraswathy, A.; Nazeer, S. S.; Francis, N.; Shenoy, S. J.; Jayasree, R. S. Multifunctional hybrid nanoconstruct of zerovalent iron and carbon dots for magnetic resonance angiography and optical imaging: An In vivo study. *Biomaterials* **2018**, *171*, 46−56.
(13) Zhang, H. Y.; Wang, Y.; Xiao, S.; Wang, H.; Wang, J. H.; Feng, L. Rapid detection of Cr(VI) ions based on cobalt(II)-doped carbon dots. *Biosens. Bioelectron.* **2017**, *87*, 46−52.
(14) Shamsipur, M.; Barati, A.; Karami, S. Long-wavelength, multicolor, and white-light emitting carbon-based dots: Achievements made, challenges remaining, and applications. *Carbon* **2017**, *124*, 429−472.
(15) Ma, Y. S.; Cen, Y.; Sohail, M.; Xu, G. H.; Wei, F. D.; Shi, M. L.; Xu, X. M.; Song, Y. Y.; Ma, Y. J.; Hu, Q. A ratiometric fluorescence universal platform based on N, Cu codoped carbon dots to detect metabolites participating in H_2O_2-generation reactions. *ACS Appl. Mater. Interfaces* **2017**, *9*, 33011−33019.
(16) Lin, T. R.; Zhong, L. S.; Chen, H.; Li, Z. H.; Song, Z. P.; Guo, L. Q.; Fu, F. F. A sensitive colorimetric assay for cholesterol based on the peroxidase-like activity of MoS_2 nanosheets. *Microchim. Acta* **2017**, *184*, 1233−1237.
(17) Huang, Y.; Tan, J.; Cui, L. J.; Zhou, Z. D.; Zhou, S. F.; Zhang, Z. H.; Zheng, R.; Xue, Y. W.; Zhang, M. X.; Li, S. S.; Zhu, N. X.; Liang, J. T.; Li, G. L.; Zhong, L. P.; Zhao, Y. X. Graphene and Au NPs co-mediated enzymatic silver deposition for the ultrasensitive electrochemical detection of cholesterol. *Biosens. Bioelectron.* **2018**, *102*, 560−567.
(18) Zhang, F. M.; Ma, P. Y.; Deng, X. Y.; Sun, Y.; Wang, X. H.; Song, D. Q. Enzymatic determination of uric acid using water-soluble CuInS/ZnS quantum dots as a fluorescent probe. *Microchim. Acta* **2018**, *185*, 499.
(19) Liu, Y. Y.; Li, H. C.; Guo, B.; Wei, L. J.; Chen, B.; Zhang, Y. Y. Gold nanoclusters as switch-off fluorescent probe for detection of uric acid based on the inner filter effect of hydrogen peroxide-mediated enlargement of gold nanoparticles. *Biosens. Bioelectron.* **2017**, *91*, 734−740.
(20) Kaushik, A.; Solanki, P. R.; Kaneto, K.; Kim, C.; Ahmad, S.; Malhotra, B. D. Nanostructured iron oxide platform for impedimetric cholesterol detection. *Electroanalysis* **2010**, *22*, 1045−1055.
(21) Yang, L. Q.; Huang, N.; Lu, Q. Q.; Liu, M. L.; Li, H. T.; Zhang, Y. Y.; Yao, S. Z. A quadruplet electrochemical platform for ultrasensitive and simultaneous detection of ascorbic acid, dopamine, uric acid and acetaminophen based on a ferrocene derivative functional Au NPs/carbon dots nanocomposite and grapheme. *Anal. Chim. Acta* **2016**, *903*, 69−80.
(22) Arya, S. K.; Solanki, P. R.; Singh, S.; Kaneto, K.; Pandey, M. K.; Datta, M.; Malhotra, B. D. Poly-(3-hexylthiophene) self-assembled monolayer based cholesterol biosensor using surface plasmon resonance technique. *Biosens. Bioelectron.* **2007**, *22*, 2516−2524.
(23) Xu, S. J.; Wang, Y. Q.; Zhou, D. Y.; Kuang, M.; Fang, D.; Yang, W. H.; Wei, S. J.; Ma, L. A novel chemiluminescence sensor for sensitive detection of cholesterol based on the peroxidase-like activity of copper nanoclusters. *Sci. Rep.* **2016**, *6*, No. 39157.
(24) Ahmad, R.; Tripathy, N.; Hahn, Y. B. High-performance cholesterol sensor based on the solution-gated field effect transistor fabricated with ZnO nanorods. *Biosens. Bioelectron.* **2013**, *45*, 281−286.
(25) Li, X.-L.; Li, G.; Jiang, Y. Z.; Kang, D. Z.; Jin, C. H.; Shi, Q.; Jin, T. F.; Inoue, K.; Todoroki, K.; Toyo'oka, T.; Min, J. Z. Human nails metabolite analysis: A rapid and simple method for quantification of uric acid in human fingernail by high-performance liquid chromatography with UV-detection. *J. Chromatogr. B: Anal. Technol. Biomed. Life Sci.* **2015**, *1002*, 394−398.
(26) Du, F.; Min, Y.; Zeng, F.; Yu, C.; Wu, S. A targeted and FRET based ratiometric fluorescent nanoprobe for imaging mitochondrial hydrogen peroxide in living cells. *Small* **2014**, *10*, 964−972.
(27) Liu, F.; Bing, T.; Shangguan, D.; Zhao, M.; Shao, N. Ratiometric fluorescent biosensing of hydrogen peroxide and hydroxyl radical in living cells with lysozyme−silver nanoclusters: Lysozyme as stabilizing ligand and fluorescence signal unit. *Anal. Chem.* **2016**, *88*, 10631−10638.
(28) Song, Y. H.; Chen, J. Y.; Hu, D. Q.; Liu, F. F.; Li, P.; Li, H. B.; Chen, S. H.; Tan, H. L.; Wang, L. Ratiometric fluorescent detection of biomakers for biological warfare agents with carbon dots chelated europium-based nanoscale coordination polymers. *Sens. Actuators, B* **2015**, *221*, 586−592.
(29) Huang, S.; Wang, L. M.; Huang, C. S.; Su, W.; Xiao, Q. Label-free and ratiometric fluorescent nanosensor based on amino-functionalized graphene quantum dots coupling catalytic G-quadruplex/hemin DNAzyme for ultrasensitive recognition of human telomere DNA. *Sens. Actuators, B* **2017**, *245*, 648−655.
(30) Liu, J. W.; Luo, Y.; Wang, Y. M.; Duan, L. Y.; Jiang, J. H.; Yu, R. Q. Graphitic carbon nitride nanosheets-based ratiometric fluorescent probe for highly sensitive detection of H_2O_2 and glucose. *ACS Appl. Mater. Interfaces* **2016**, *8*, 33439−33445.
(31) Xiao, Q.; Liang, Y.; Zhu, F. W.; Lu, S. Y.; Huang, S. Microwave-assisted one-pot synthesis of highly luminescent N-doped carbon dots for cellular imaging and multi-ion probing. *Microchim. Acta* **2017**, *184*, 2429−2438.
(32) Lan, M. H.; Di, Y. F.; Zhu, X. Y.; Ng, T. W.; Xia, J.; Liu, W. M.; Meng, X. M.; Wang, P. F.; Lee, C. S.; Zhang, W. J. A carbon dot-based fluorescence turn-on sensor for hydrogen peroxide with a photo-induced electron transfer mechanism. *Chem. Commun.* **2015**, *51*, 15574−15577.

DOI: 10.1021/acsomega.9b00874
ACS Omega 2019, 4, 9333−9342

(33) Wang, R. X.; Wang, X. F.; Sun, Y. M. One-step synthesis of self-doped carbon dots with highly photoluminescence as multifunctional biosensors for detection of iron ions and pH. *Sens. Actuators, B* **2017**, *241*, 73−79.
(34) Atchudan, R.; Edison, T. N. J. I.; Sethuraman, M. G.; Lee, Y. R. Efficient synthesis of highly fluorescent nitrogen-doped carbon dots for cell imaging using unripe fruit extract of *Prunus mume*. *Appl. Surf. Sci.* **2016**, *384*, 432−441.
(35) Yu, C. Y.; Xuan, T. T.; Chen, Y. W.; Zhao, Z. J.; Liu, X. X.; Lian, G. H.; Li, H. L. Gadolinium-doped carbon dots with high quantum yield as an effective fluorescence and magnetic resonance bimodal imaging probe. *J. Alloys Compd.* **2016**, *688*, 611−619.
(36) Hu, T. Y.; He, J.; Zhang, S. M.; Mei, X.; Zhang, W. K.; Liang, R. Z.; Wei, M.; Evans, D. G.; Duan, X. An ultrathin photosensitizer for simultaneous fluorescence imaging and photodynamic therapy. *Chem. Commun.* **2018**, *54*, 5760−5763.
(37) Hou, J.; Wang, L.; Zhang, P.; Xu, Y.; Ding, L. Facile synthesis of carbon dots in an immiscible system with excitation-independent emission and thermally activated delayed fluorescence. *Chem. Commun.* **2015**, *51*, 17768−17771.
(38) Huang, S.; Yang, E. L.; Yao, J. D.; Liu, Y.; Xiao, Q. Carbon dots doped with nitrogen and boron as ultrasensitive fluorescent probes for determination of α-glucosidase activity and its inhibitors in water samples and living cells. *Microchim. Acta* **2018**, *185*, 394.
(39) Huang, S.; Yang, E. L.; Yao, J. D.; Liu, Y.; Xiao, Q. Red emission nitrogen, boron, sulfur co-doped carbon dots for "on-off-on" fluorescent mode detection of Ag^{+} ions and L-cysteine in complex biological fluids and living cells. *Anal. Chim. Acta* **2018**, *1035*, 192−202.
(40) Zeng, Y. W.; Ma, D. K.; Wang, W.; Chen, J. J.; Zhou, L.; Zheng, Y. Z.; Yu, K.; Huang, S. M. N, S Co-doped carbon dots with orange luminescence synthesized through polymerization and carbonization reaction of amino acids. *Appl. Surf. Sci.* **2015**, *342*, 136−143.
(41) Ma, Y.; Chen, Y. L.; Liu, J. J.; Han, Y. X.; Ma, S. D.; Chen, X. G. Ratiometric fluorescent detection of chromium(VI) in real samples based on dual emissive carbon dots. *Talanta* **2018**, *185*, 249−257.
(42) Liu, Y.; Duan, W. X.; Song, W.; Liu, J. J.; Ren, C. L.; Wu, J.; Liu, D.; Chenm, H. L. Red emission B, N, S-co-doped carbon dots for colorimetric and fluorescent dual mode detection of Fe^{3+} ions in complex biological fluids and living cells. *ACS Appl. Mater. Interfaces* **2017**, *9*, 12663−12672.
(43) Gupta, V.; Chaudhary, N.; Srivastava, R.; Sharma, G. D.; Bhardwaj, R.; Chand, S. Luminscent graphene quantum dots for organic photovoltaic devices. *J. Am. Chem. Soc.* **2011**, *133*, 9960−9963.
(44) Ju, B.; Wang, Y.; Zhang, Y. M.; Zhang, T.; Liu, Z. H.; Li, M. J.; Zhang, S. X. A. Photostable and low-toxic yellow-green carbon dots for highly selective detection of explosive 2,4,6-trinitrophenol based on the dual electron transfer mechanism. *ACS Appl. Mater. Interfaces* **2018**, *10*, 13040−13047.
(45) Chen, S.; Yu, Y. L.; Wang, J. H. Inner filter effect-based fluorescent sensing systems: A review. *Anal. Chim. Acta* **2018**, *999*, 13−26.
(46) Liu, H.; Xu, C.; Bai, Y.; Liu, L.; Liao, D.; Liang, J.; Liu, L.; Han, H. Interaction between fluorescein isothiocyanate carbon dots: Inner filter effect and fluorescence resonance energy transfer. *Spectrochim. Acta, Part A* **2017**, *171*, 311−316.
(47) Wang, W. T.; Ji, X.; Kapur, A.; Zhang, C. Q.; Mattoussi, H. A multifunctional polymer combining the imidazole and zwitterion motifs as a biocompatible compact coating for quantum dots. *J. Am. Chem. Soc.* **2015**, *137*, 14158−14172.
(48) Hu, Y.; Zhang, Z. Determination of free cholesterol based on a novel flow-injection chemiluminescence method by immobilizing enzyme. *Luminescence* **2008**, *23*, 338−343.

DOI: 10.1021/acsomega.9b00874
ACS Omega 2019, 4, 9333−9342